Fractional-order chaotic system with hyperbolic function

G Gugapriya[1], Prakash Duraisamy[2], Anitha Karthikeyan[2] and B Lakshmi[1] (iD)

Abstract

In this article, we study bistability, multiscroll, and symmetric properties of fractional-order chaotic system with cubic nonlinearity. The system is configured with hyperbolic function consisting of a parameter "*g*." By varying the parameter "*g*," the dynamical behavior of the system is investigated. Multistability and multiscroll are identified, which makes the system suitable for secure communication applications. When the system is treated as fractional order, for the same parameter values and initial conditions and when the fractional order is varied from 0.96 to 0.99, multiscroll property is obtained. Symmetric property is obtained for the order of 0.99. The fractional system holds only single scroll until 0.965 order and when the order increases to more than 0.99, it is having two-scroll attractor. This property opens a variety of applications for the systems, especially in secure communication. Adaptive synchronization of the system using sliding mode control scheme is presented. For implementing the fractional-order system in field-programmable gate array, Adomian decomposition method is used, and the register-transfer level schematic of the system is presented.

Introduction

Designing chaotic systems with more complex dynamics has been of great interest to the researchers.[1–6] Dynamical systems with multiscroll attractors can present more complex dynamics than general chaotic systems with mono-scroll attractors. Chaotic system with multiscroll attractors found its significance in secure communication because of the system complexity which greatly improves the encryption performance.[7] Various methods have been proposed to generate multiscroll attractors.[8–15] The introduction of a family of *n*-scroll chaotic attractors by Suykens and Vandewalle[16] using quasi-linear function method is identified as one of the methods to strengthen the complexity of chaotic system. After the formulation of a generalized *n*-double scroll Chua's circuit using three-state controlled cellular neural network, designing multiscroll chaotic system became a hot topic in chaotic research field.[17,18]

The generation of multiscroll attractors by controlling the equilibrium point of a system is discussed in Ontañón-García et al.[19] Time-delayed hyperchaotic system having multiscroll attractors with multiple positive Lyapunov exponents (LEs) is proposed in Wang et al.[20] A chaotic oscillator capable of generating *n*-scroll chaos with multiple-cycle nonlinear transconductor is reported in Salama et al.[21] Microcontroller-based circuit realization of a four-dimensional multiscroll hyperchaotic system is proposed in Sun et al.[22] The generation and application of one- and two-dimensional

[1]Vellore Institute of Technology, Chennai, India
[2]Center for Nonlinear Dynamics, Defence University, Bishoftu, Ethiopia

Corresponding author:
B Lakshmi, Vellore Institute of Technology, Vandalur-Kelambakkam Road, Chennai 600127, Tamil Nadu, India.
Email: lakshmi.b@vit.ac.in

(2D) multiscroll chaotic systems in an encryption technique is given in Radwan and Abd-El-Hafiz.[23] Cellular neural network–based chaotic model for generating multiscroll attractors with hyperbolic tangent function series is proposed in Günay and Altun.[24] Introducing hyperbolic function is one successful method to enhance the number of scrolls present in the system.

Fractional order offers a novel modeling approach for systems with extraordinary dynamical properties by introducing the notion of a derivative of non-integer (fractional) order. Fractional calculus is found especially useful in system theory and automatic control, where fractional differential equations are used to obtain more accurate models of dynamic systems.[25] It also develops new control strategies and enhances the characteristics of control loops. Fractional-order systems have recently emerged as another platform capable of demonstrating multiscroll chaotic attractors.[26,27] Such systems can give rise to chaos even though the total order is less than 3 (however, greater than 2).[28] The chaotic systems with rich dynamic properties can find its application in cryptosystem.[29–31] Complete analysis and engineering applications of a mega stable nonlinear oscillator are given in the literature.[32]

In this article, hyperbolic function is introduced in a cubic nonlinear system to achieve multiscroll, symmetricity, and bistability, which increases the complexity of the system, and hence the system can be used in secure communications. In addition, we bring out a new way of finding multiscroll property by varying only the fractional order "q," which is not mentioned in any recent literatures.

An autonomous chaotic system with cubic nonlinearity[33] is investigated for nonlinear properties. The state-space equation is given in equation (1). The system showed chaotic behavior for particular values of parameters

$$\begin{aligned}
\dot{x}_1 &= -ax_1 + bx_2x_3 \\
\dot{x}_2 &= -cx_2^3 + dx_1x_3 \\
\dot{x}_3 &= ex_3 - fx_1x_2
\end{aligned} \quad (1)$$

Multiscroll property is analyzed in system[33] by varying the parameters a and c. Special properties like multistability and symmetricity are not analyzed in system.[33] Fractional-order form is also not analyzed. If the chaotic system is rich in dynamics, it will be more suitable for secure communications.

In this work, we investigated the influence of hyperbolic function on dynamical behaviors of the system (1) and also analyzed special properties. Furthermore, we formulated fractional-order form of the system using Grunwald–Letnikov (G-L) method for refining the analysis. The article is organized into five sections. The second section provides the details and configuration about the chaotic system with cubic nonlinearity and hyperbolic function. The third section deals with the analysis of the integer system for various dynamical properties. The fourth section provides the generation of fractional-order chaotic system with hyperbolic function and its dynamical behaviors. The fifth section discusses the synchronization scheme, and the last section provides field-programmable gate array (FPGA) implementation.

Three-dimensional chaotic system with cubic nonlinearity and hyperbolic function

In this article, we modified the system (1) by introducing a hyperbolic function $p_1 \tanh(x_2 + g)$. Chaotic attractor is obtained when $a = 2$, $b = 6$, $c = 6$, $d = 3$, $e = 3$, $f = 1$, $p_1 = 1$, and $g = 2$, and the chosen initial conditions are $[x_1(0), x_2(0), x_3(0)] = [0.1, 0.1, 0.6]$.

When the hyperbolic function is introduced in first state with the parameter $g = -3$ and for the initial conditions $[0.1, -0.1, -0.6]$, it shows a double-scroll attractor which is shown in Figure 1. When introduced in the second state, with parameters $p_1 = -1$ and $g = 3$ and initial conditions $[0.1, -0.1, -0.6]$, it shows four scroll which is shown in Figure 2. While in the third state with parameters $p_1 = 1$ and $g = 3$ and initial conditions $[0.1, 0.1, 0.6]$, it shows single scroll which is shown in Figure 3. Thus, we can confirm that the system holds multiscroll property.

We further investigated by varying the parameters "p_1" and "g", with hyperbolic function in third state. We observed multi scroll property while varying the parameter "g". This confirms that the parameter "g" plays a major role in the behavior of the system.

Dynamic analysis of the system

$$\begin{aligned}
\dot{x}_1 &= -ax_1 + bx_2x_3 \\
\dot{x}_2 &= -cx_2^3 + dx_1x_3 \\
\dot{x}_3 &= ex_3 - fx_1x_2 + p_1 \tanh(x_2 + g)
\end{aligned} \quad (2)$$

Chaotic attractor is obtained when $a = 2$, $b = 6$, $c = 6$, $d = 3$, $e = 3$, $f = 1$, $p_1 = 1$, and $g = 2$, and the chosen initial conditions are $[x_1(0), x_2(0), x_3(0)] = [0.1, 0.1, 0.6]$.

Equilibrium point and stability

Equilibrium points are obtained by solving $\dot{x}_1 = 0$, $\dot{x}_2 = 0$, and $\dot{x}_3 = 0$

$$\begin{aligned}
0 &= -ax_1 + bx_2x_3 \\
0 &= -cx_2^3 + dx_1x_3 \\
0 &= ex_3 - fx_1x_2 + p_1 \tanh(x_2 + g)
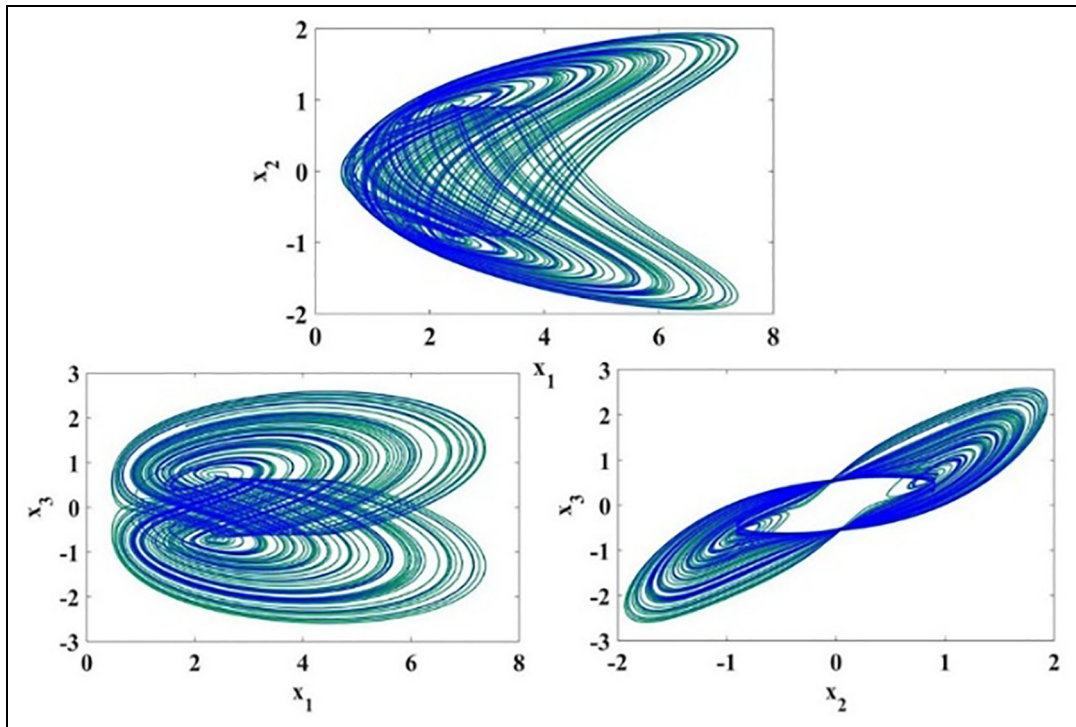\end{aligned} \quad (3)$$

Figure 1. Phase portraits of cubic nonlinear system with $p_1 \tanh(x_2 + g)$ function in first state.
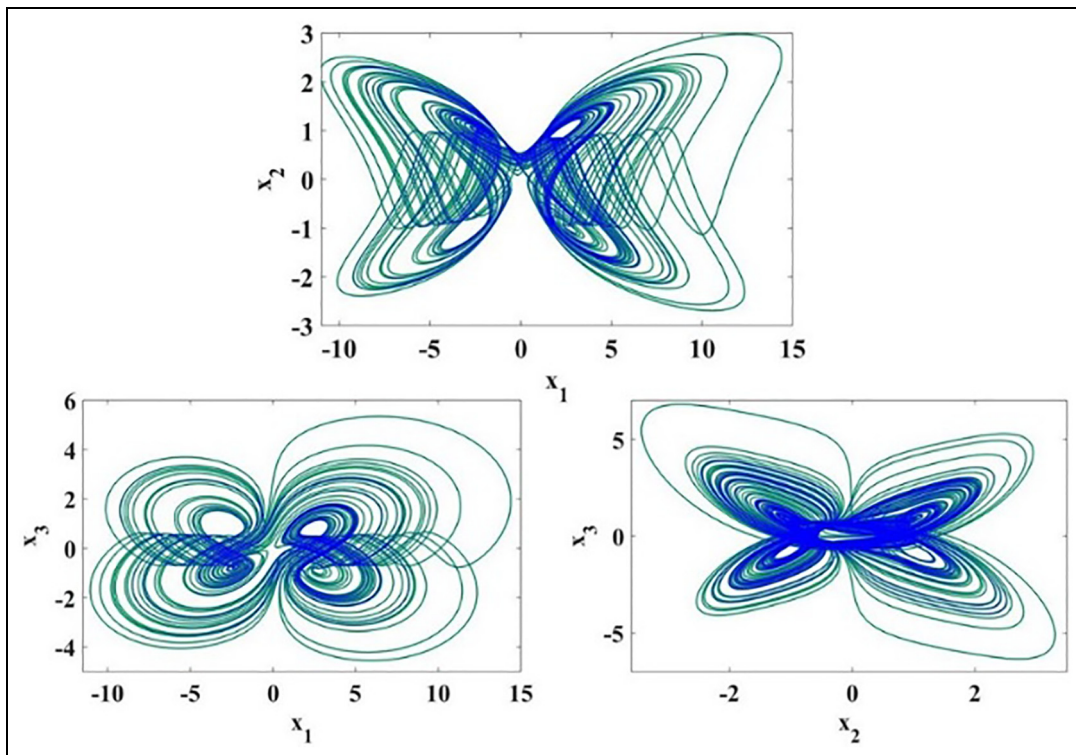

Figure 2. Phase portraits of cubic nonlinear system with $p_1 \tanh(x_2 + g)$ function in second state.

The equilibrium points are $x_1 = -2.0925e - 42$, $x_2 = 1.0325e - 41$, and $x_3 = -0.3213$. Jacobian matrix is formulated from the state space equations and is given below
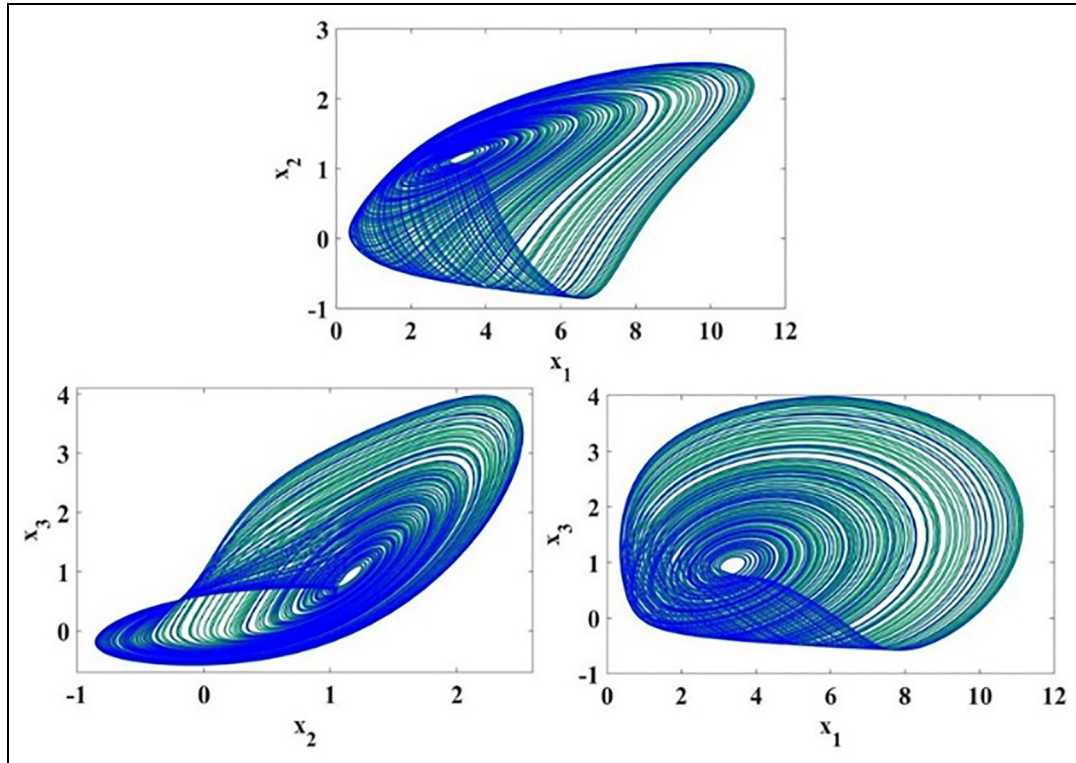
Figure 3. Phase portraits of cubic nonlinear system with $p_1 \tanh(x_2 + g)$ function in third state.

$$J = \begin{bmatrix} -a & bx_3 & bx_2 \\ dx_3 & -3cx_2^2 & dx_1 \\ -fx_2 & -fx_1 - p_1 \tan(g + x_2)^2 - 1 & e \end{bmatrix}$$

The corresponding characteristic equation for the above Jacobian matrix is $\lambda^3 - \lambda^2 - 7.8582\lambda + 5.5746 = 0$. The Eigenvalues are $\lambda_1 = -2.6906$, $\lambda_2 = 0.6906$, and $\lambda_3 = 3.0000$. The two positive Eigenvalues prove that the equilibrium point is unstable.

LEs

LEs of a nonlinear system define the convergence and divergence of the states. Although there are different methods, we used the famous method proposed by Wolf et al.[34] The LEs of the system are numerically found as $LE_1 = 0.4002$, $LE_2 = -0.0003$, and $LE_3 = -11.6537$. The sum of LEs is negative, which shows the system is dissipative. One positive LE confirms the existence of chaos in the system.

As mentioned before, the parameter "g" varies from −5 to + 5, and LEs are plotted in Figure 4. The system shows bistability as can be seen from Figure 5. The bifurcation diagram is obtained by plotting local maxima of the coordinate "x_2" in terms of the parameter "g" which is increased (or decreased) in tiny steps. The existence of multistability can be confirmed by
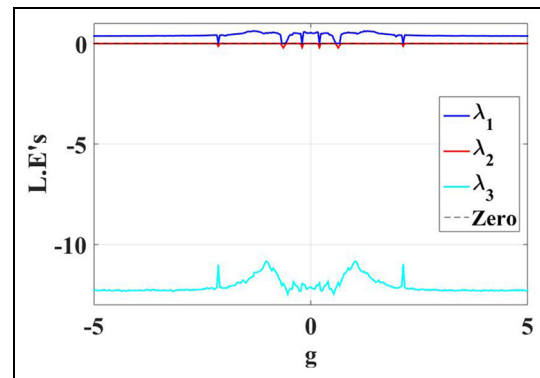

Figure 4. Lyapunov exponent spectrum for "g" values from −5 to + 5.

comparing the forward (dark blue color) and backward (red color) bifurcation diagrams as shown in Figure 5.

Phase portraits

The phase portraits of system (2) are plotted for the simulation time of 1000. The numerical simulation is carried out for parameter values $a = 2$, $b = 6$, $c = 6$, $d = 3$, $e = 3$, $f = 1$, and $p_1 = 1$, for the initial conditions [0.1, 0.1, 0.6]. Figure 6 shows the phase portraits of the system, where four-scroll attractor is observed, for $g = 0$. The system generates four-scroll attractor
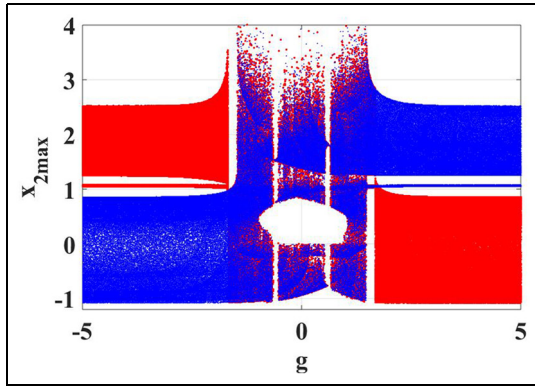
Figure 5. Bifurcation of parameter "*g*" for different initial conditions.

without the hyperbolic function. Figure 7 shows the phase portraits of the system for $g = 1.2$, where two-scroll attractor is noted. When the parameter "*g*" value is increased to 2, it produces single-scroll attractor as shown in Figure 8. When the initial condition is changed to $[0.1, -0.1, 0.6]$, a single-scroll attractor is observed with symmetricity as shown in Figure 9.

Fractional-order chaotic system with cubic nonlinearity and hyperbolic function

In this section, we derive the fractional-order model of the chaotic system with cubic nonlinearity and

hyperbolic function. There are three generally used definitions of the fractional-order differential operator, namely, G-L, Riemann–Liouville (R-L), and Caputo.[35,36]

We used the G-L definition, which can be defined as

$$
\begin{aligned}
D_{t}^{q}f(t) &= \lim_{h \to 0}\left\{ \frac{1}{h^{q}}\sum_{j=0}^{\left[\frac{t-q}{h}\right]}(-1)^{j}\binom{q}{j}f(t-jh) \right\} \\
&= \lim_{h \to 0}\left\{ \frac{1}{h^{q}}\Delta_{h}^{q}f(t) \right\}
\end{aligned}
\tag{4}
$$

where a and t are limits of the fractional-order equation, Δ_{h}^{q} is generalized difference, h is the step size, and q is the fractional-order of the differential equation.

For numerical calculations, the above equation is modified as

$$
{}_{t-L}D_{t}^{q}f(t) = \lim_{h \to 0}\left\{ \frac{1}{h^{q}}\sum_{j=0}^{N(t)}b_{j}f(t-jh) \right\}
\tag{5}
$$

Theoretically, fractional-order differential equations use infinite memory. Hence, for numerical calculations or simulations of the fractional-order equations, we have to use finite memory principle

$$
N(t) = \min\left\{ \left[\frac{t}{h}\right], \left[\frac{L}{h}\right] \right\}
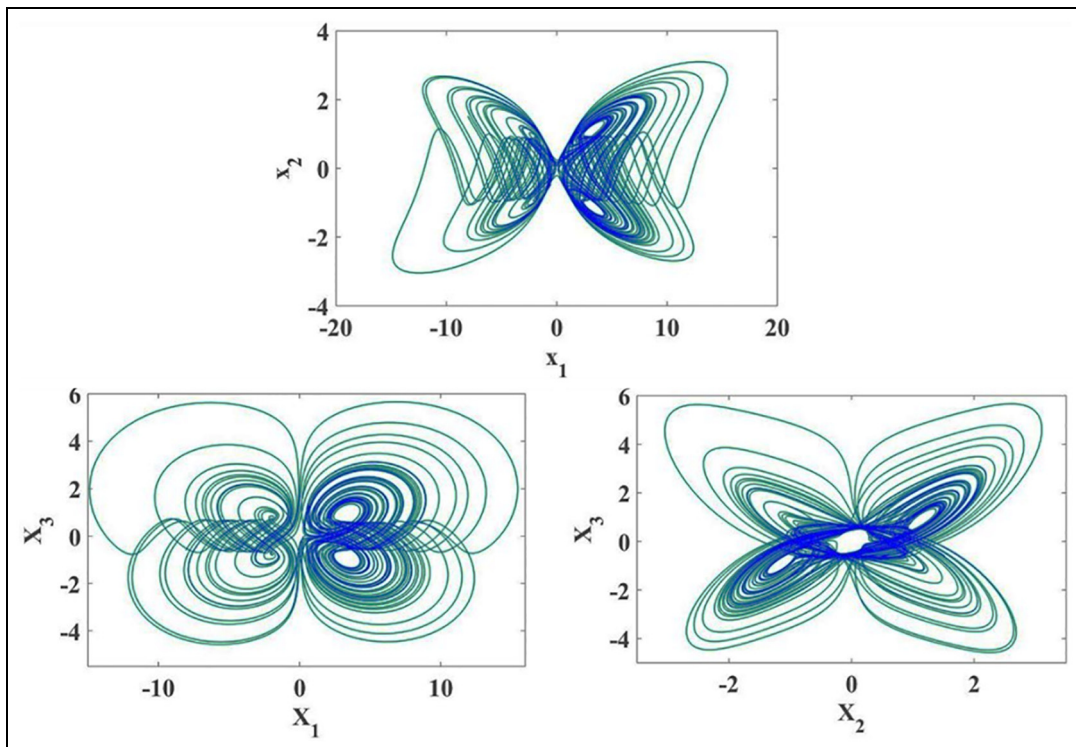\tag{6}
$$

Figure 6. Phase portraits for $g = 0$ (four-scroll attractor).
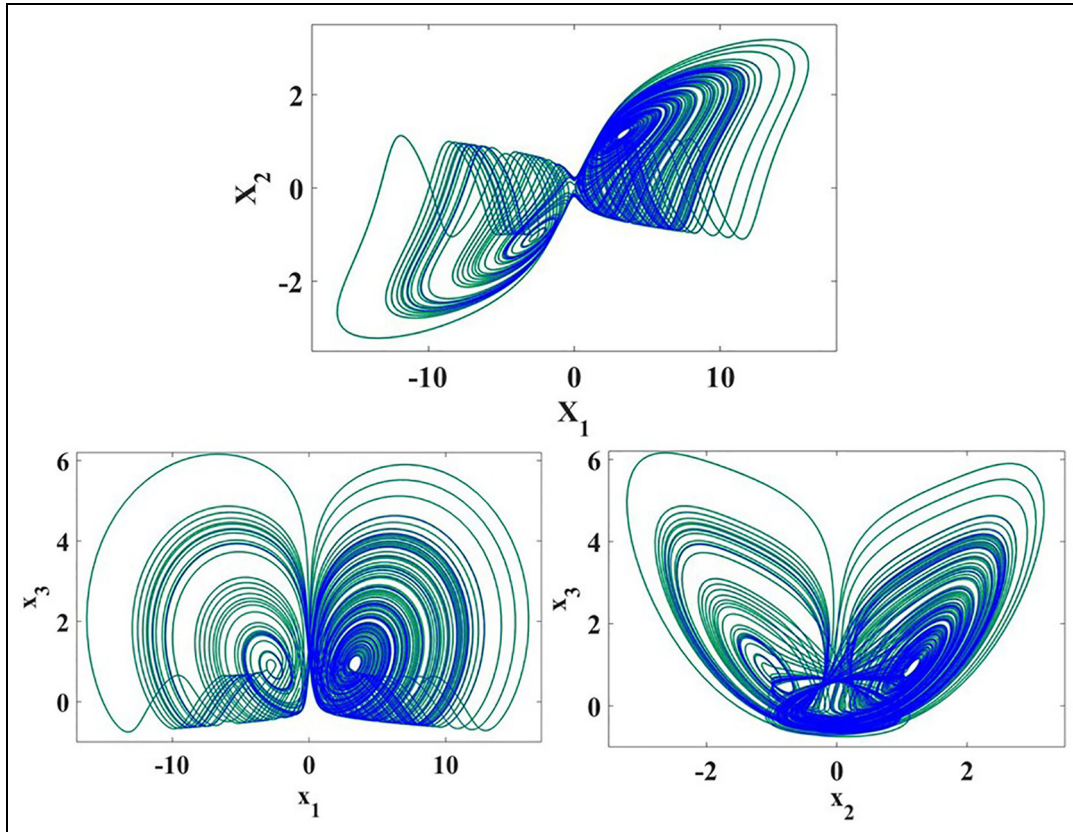
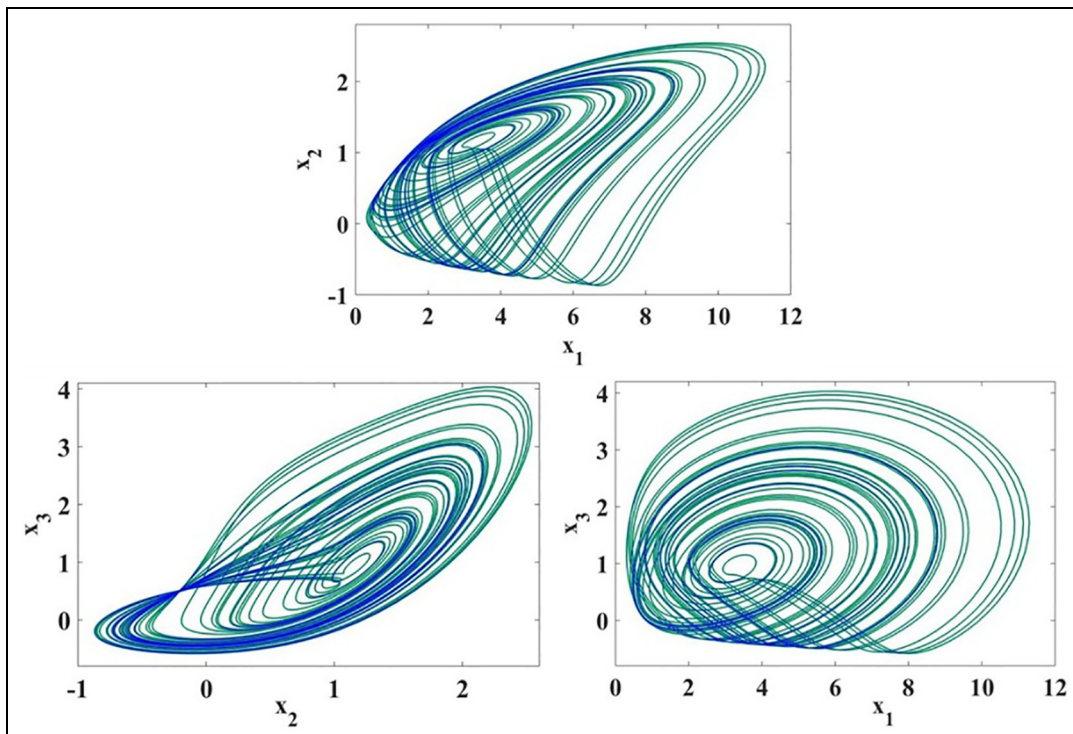**Figure 7.** Phase portraits for *g* = 1.2 (two-scroll attractor).

Figure 8. Phase portraits for *g* = 2 (single-scroll attractor) for initial conditions [0.1, 0.1, 0.6].
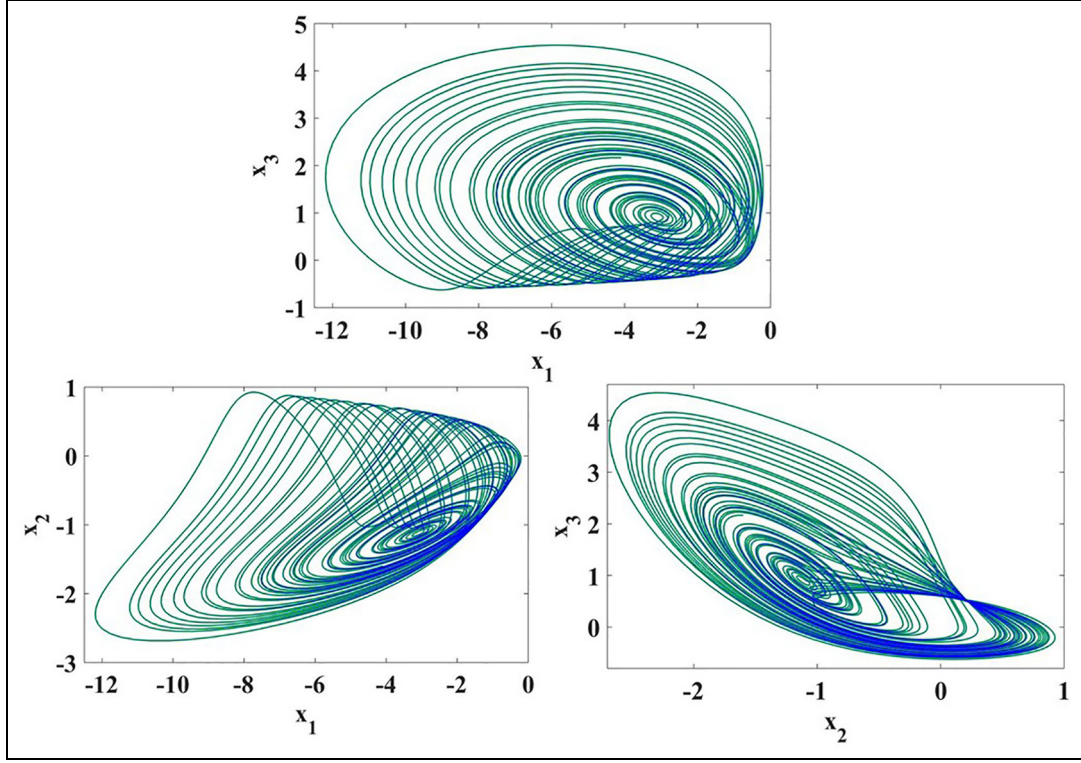
Figure 9. Phase portraits for $g = 2$ for initial conditions [0.1, –0.1, 0.6].

where L is the memory length and h is the time sampling.

The binomial coefficients required for the numerical simulation are calculated as

$$b_j = \left(1 - \frac{a + q}{j}\right) b_{j-1} \tag{7}$$

Irrespective of the importance of the function $f(t)$ near the lower terminal $t = a$, Volterra proposed the short memory principle for simplification. Sometimes, short memory principle can be regarded as a structural property of the differential operator.

For the G-L definition, the values of binomial coefficients near the starting point $t = 0$ are small enough to be neglected or omitted for large t values. So, the short memory principle is considered as the behavior of the function $f(t)$ only in the interval $[t - L, t]$, where L is the length of the memory.[37]

Short memory principle

If $|f(t)| < M$, $\nabla t > 0$, then the error ε is bounded by

$$|\varepsilon| < \frac{M}{L^q |\Gamma(1 - q)|} \tag{8}$$

When $q = 0$

$$|\varepsilon| < |_{t_0}D_t^q f(t) - {}_{t-L}D_t^q f(t)| = |_{t_0}D_{t-L}^q f(t)| \tag{9}$$

$$|\varepsilon| < \left| \int_{t_0}^{t-L} \frac{(t - \tau)^{-q-1}}{\Gamma(-q)} f(\tau) d\tau \right| \leq \left| \int_{t_0}^{t-L} \frac{(t - \tau)^{-q-1}}{\Gamma(-q)} M d\tau \right| \tag{10}$$

$$= \left| \frac{M}{\Gamma(-q)} \left[\frac{-1}{q} (t - \tau)^{-q} \right]_{t_0}^{t-L} \right| = \left| \frac{M[(t - t_0)^{-q} - L^{-q}]}{\Gamma(1 - q)} \right| \tag{11}$$

It cannot be a useful bound, as it grows with $t - t_0$ and becomes very large. When $q > 0$

$$|\varepsilon| \leq \left| \frac{d^{[q]}}{dt^{[q]}} {}_{t_0}D_t^{q-[q]} f(t) - \frac{d^{[q]}}{dt^{[q]}} {}_{t-L}D_t^{q-[q]} f(t) \right| \tag{12}$$

$$= \left| \frac{d^{[q]}}{dt^{[q]}} {}_{t_0}D_{t-L}^{q-[q]} f(t) \right| \tag{13}$$

$$|\varepsilon| \leq \left| \frac{d^{[q]}}{dt^{[q]}} \frac{M\left[(t - t_0)^{-q + [q]} - L^{-q + [q]} \right]}{\Gamma(1 - q + [q])} \right| \tag{14}$$

Since

$$_0D_t^q t^\lambda = \frac{\Gamma(\lambda + 1)}{\Gamma(\lambda - q + 1)} t^{\lambda - q} \; ; t \in \mathbb{R}^+ \; ; \lambda \notin \mathbb{Z}^- \tag{15}$$
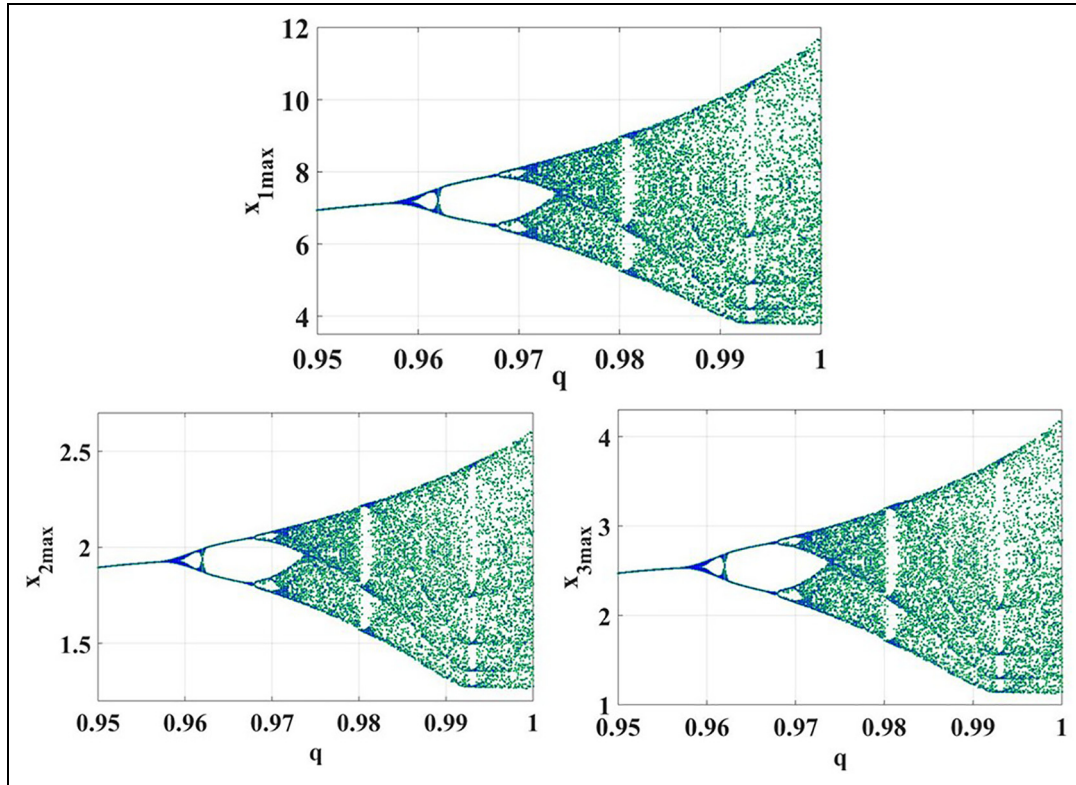
Figure 10. Fractional order bifurcation.

we can write

$$|\varepsilon| \leqslant \left| \frac{M[(t-t_0)^{-q} - \Gamma(1-q+[q])]}{\Gamma(1-q+[q]-[q])\Gamma(1-q+[q])} \right|$$
$$= \frac{M}{(t-t_0)^{-q}|\Gamma(1-q)|} \tag{16}$$

Since $t - t_0 > 0$, which implies

$$(t-t_0)^q > L^q \Rightarrow \frac{1}{(t-t_0)^q} < \frac{1}{L^q} \tag{17}$$

$$|\varepsilon| \leqslant \frac{M}{(t-t_0)^q|\Gamma(1-q)|} < \frac{M}{L^q|\Gamma(1-q)|} \tag{18}$$

Thus to ensure that the absolute value of error ε should not be larger than a certain value, the memory length must satisfy

$$L \geqslant \left(\frac{M}{|\varepsilon\Gamma(1-q)|} \right)^{-q} ; \quad q > 0 \tag{19}$$

Using equations (4) to (7), we derive the fractional-order chaotic system with cubic nonlinearity and hyperbolic function

$$\frac{d^q x_1}{dt^q} = -ax_1 + bx_2 x_3$$
$$\frac{d^q x_2}{dt^q} = -cx_2^3 + dx_1 x_3 \tag{20}$$
$$\frac{d^q x_3}{dt^q} = ex_3 - fx_1 x_2 + p_1 \tanh(x_2 + g)$$

Fractional-order bifurcation

As can be seen from Figure 10, for the change in the fractional order "q" with parameter values $a = 2$, $b = 6$, $c = 6$, $d = 3$, $e = 3$, $f = 1$, $p_1 = 1$, and $g = 1.2$, bifurcation of the system (20) shows that the system chaotic oscillations starts when $q = 0.972$. Figure 11 shows the phase portrait of the periodic oscillation when the order q is 0.954. Until $q = 0.97$, we can see the period doubling range. Figure 12 shows two-period oscillation for the order $q = 0.965$. Figure 13 shows the clear single-scroll chaotic attractor.

Symmetric property

The fractional-order system (20) is investigated for symmetric property, for order $q = 0.99$. For same parameter values and initial conditions [0.1, 0.1, 0.6],
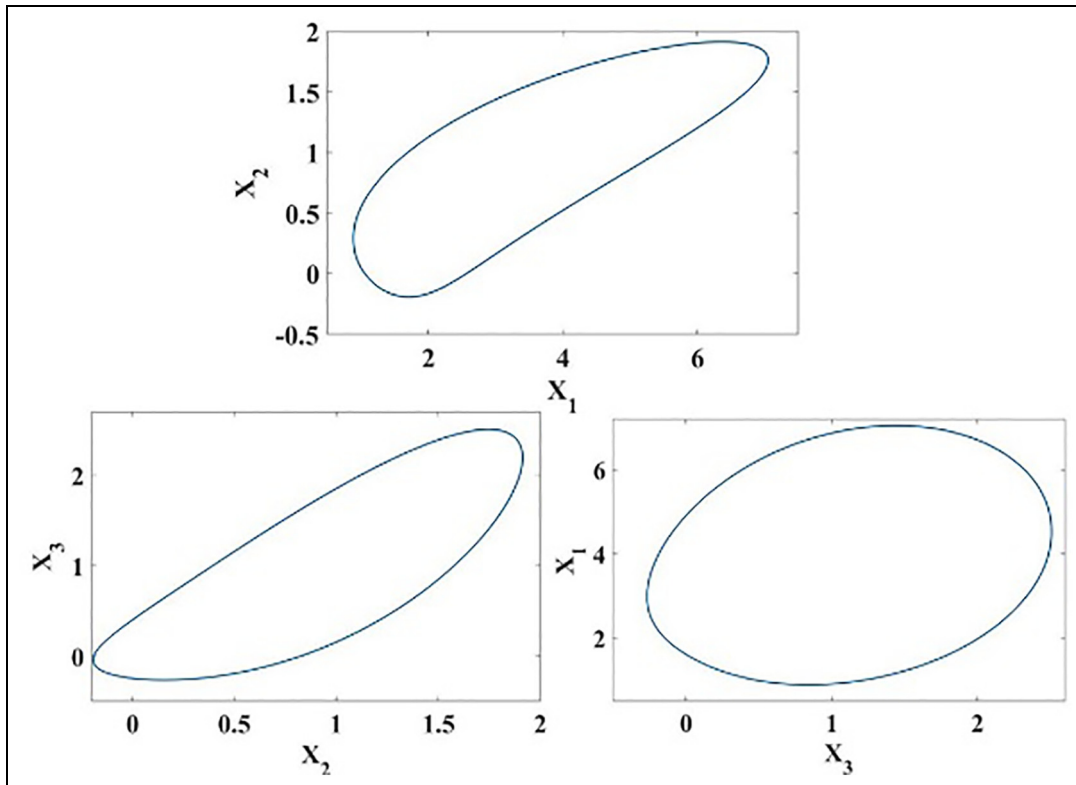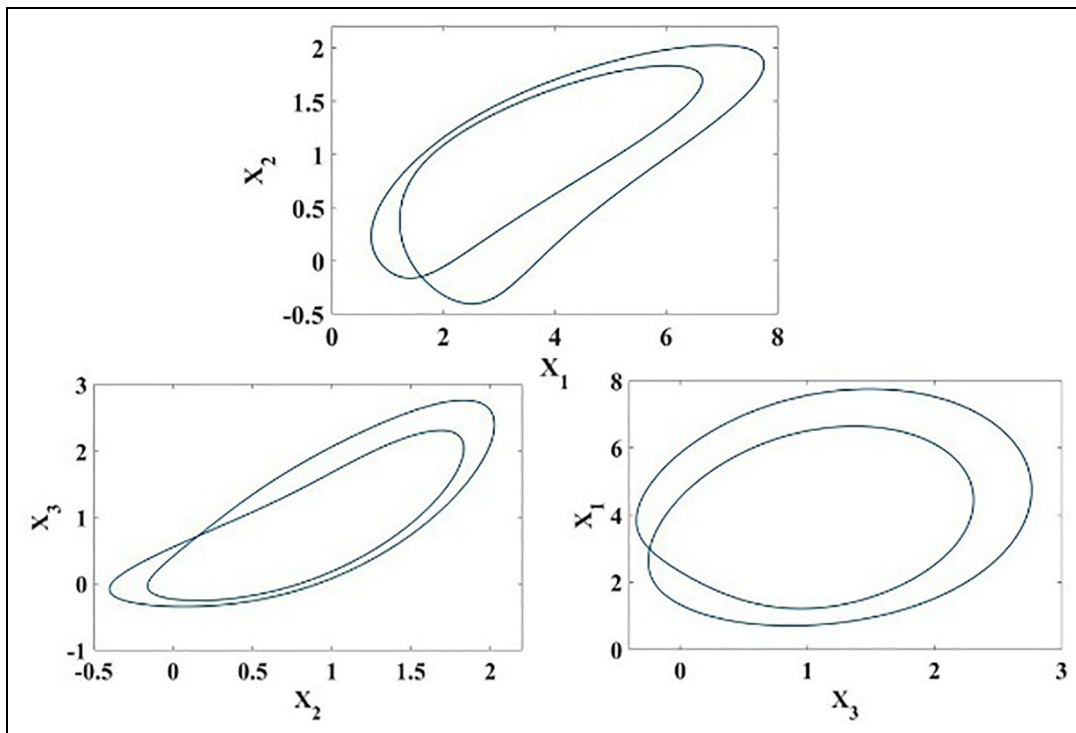
Figure 11. Phase portrait for $q = 0.954$.

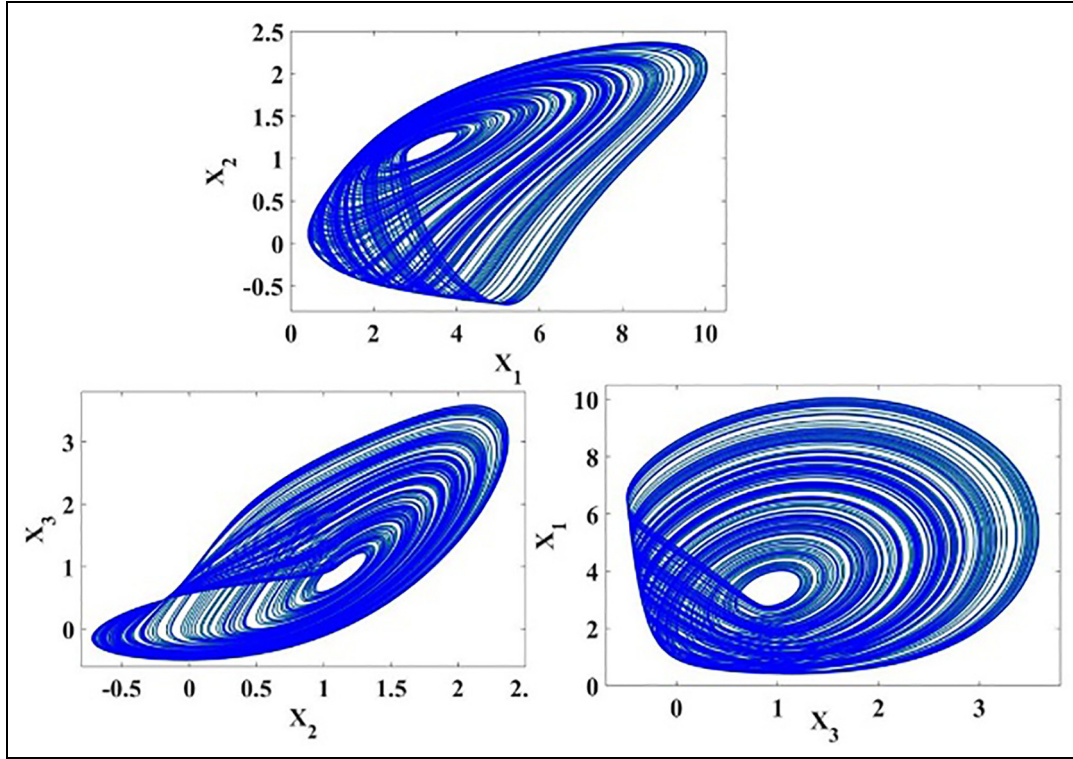**Figure 12.** Phase portrait for $q = 0.965$.

Figure 13. Phase portrait for $q = 0.99$.

single-scroll attractor is plotted in dark blue color, and for initial conditions $[0.1, -0.1, 0.6]$, symmetric single-scroll attractor is plotted in red color. Figure 14 shows that the system exhibits symmetric property for the fractional-order system.

Multiscroll property

Even though the integer order treatment of the system for various "g" values shows multiscroll, interestingly we could observe bistability in varying the order itself. For $g = 1.2$ and order $q = 0.96$, the system shows single scroll (Figure 15). But for same "g" value when order reaches to 0.99, we could observe clear two-scroll attractor (Figure 16). Previously, in Figure 7, we showed the integer order system having two-scroll attractor. It can be observed that for the fractional system up to fractional order 0.965, the system holds single scroll, and when the order is increased above 0.99, it is having two-scroll attractor.

Adaptive synchronization of the system using sliding mode control

Various synchronization techniques for multiscroll attractors are discussed in Li and colleagues.[38,39]

The sliding control methodology is found to be effective technique for dealing dynamic uncertainty.[40,41] In this section, we are using adaptive sliding mode control method to derive for synchronization of the system (2).

The master system is taken as

$$\begin{aligned}
\dot{x}_m &= -ax_m + by_m z_m \\
\dot{y}_m &= -cy_m^3 + dx_m z_m \\
\dot{z}_m &= ez_m - fx_m y_m + p\tanh(y_m + g)
\end{aligned} \tag{21}$$

The slave system with controllers is

$$\begin{aligned}
\dot{x}_s &= -ax_s + by_s z_s + u_x \\
\dot{y}_s &= -cy_s^3 + dx_s z_s + u_y \\
\dot{z}_s &= ez_s - fx_s y_s + p\tanh(y_s + g) + u_z
\end{aligned} \tag{22}$$

Synchronization errors can be

$$\begin{aligned}
e_i &= i_s - i_m \\
e_x &= x_s - x_m \\
e_y &= y_s - y_m \\
e_z &= z_s - z_m
\end{aligned} \tag{23}$$

Error dynamics are derived by differentiating the synchronization errors

$$\begin{aligned}
\dot{e}_x &= -\hat{a}x_s + \hat{b}y_s z_s + ax_m - by_m z_m + u_x \\
\dot{e}_y &= -\hat{c}y_s^3 + \hat{d}x_s z_s + cy_m^3 - dx_m z_m + u_y \\
\dot{e}_z &= \hat{e}z_s - \hat{f}x_s y_s + \hat{p}\tanh(y_s + g) \\
&\quad - ez_m + fx_m y_m - p\tanh(y_m + g) + u_z
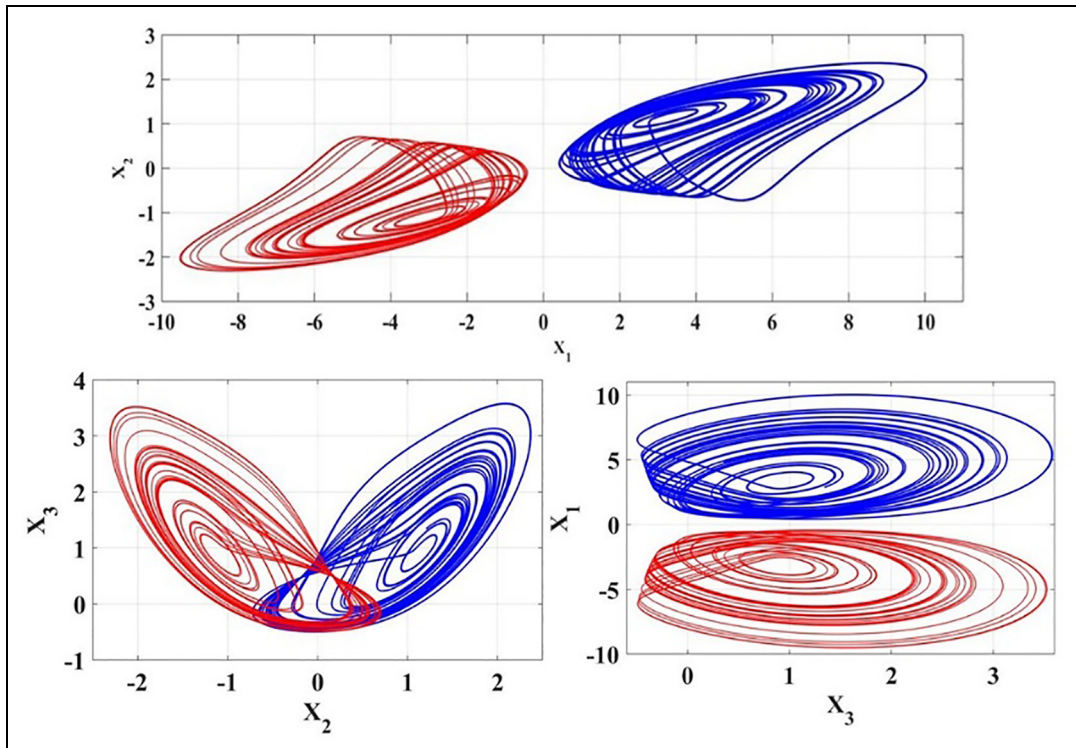\end{aligned} \tag{24}$$

Figure 14. Phase portrait for $q = 0.99$ showing symmetric property with initial conditions [0.1, 0.1, 0.6] is given in blue color and with initial conditions [0.1, –0.1, 0.6] is given in red color.
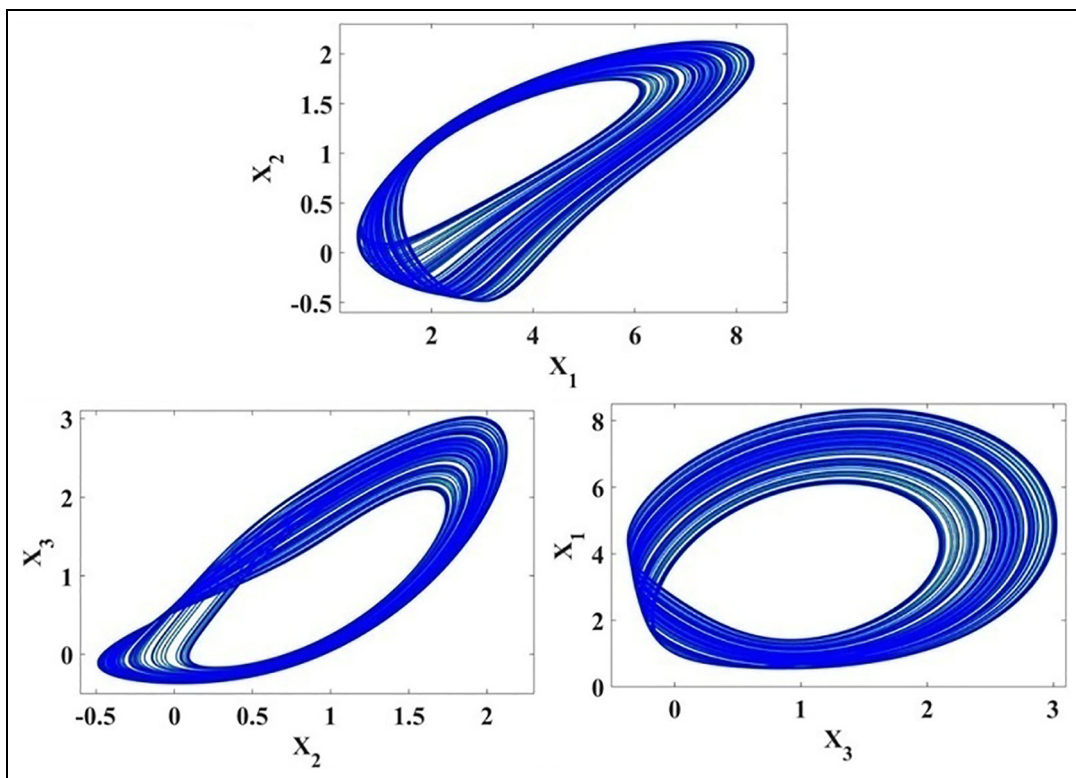

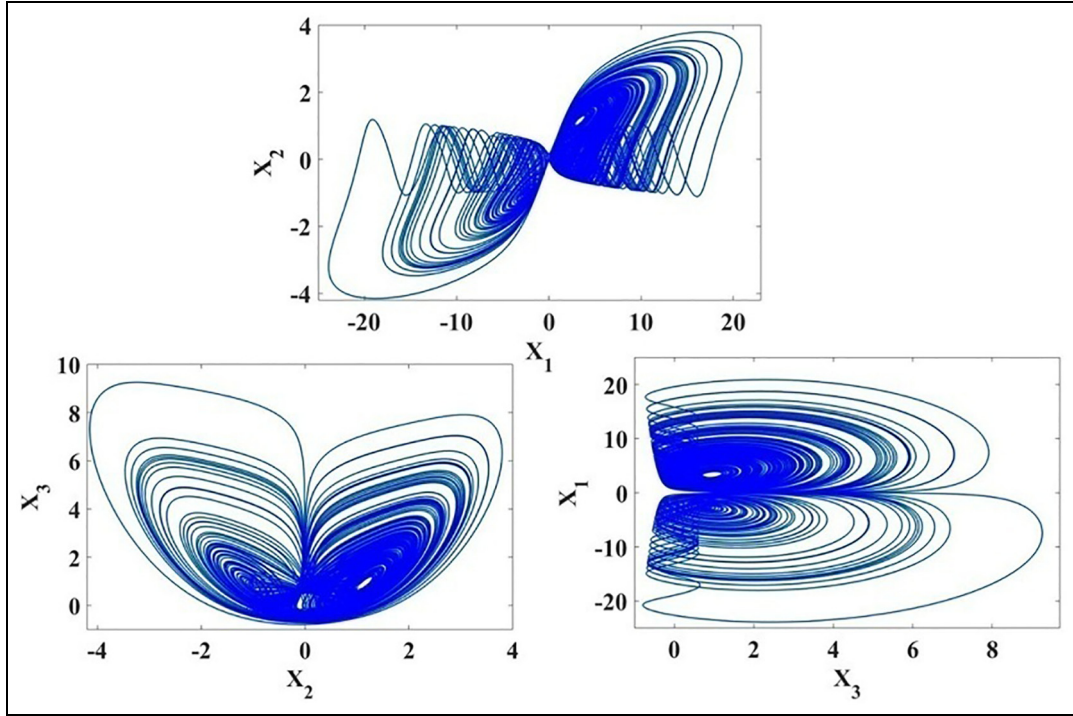**Figure 15.** Single-scroll attractor $g = 1.2$, $q = 0.96$.

Figure 16. Double-scroll attractor $g = 1.2$, $q = 0.99$.

In $\dot{e}_x$, add and subtract $-\hat{a}x_m$ and $\hat{b}y_m z_m$

$$
\begin{aligned}
\dot{e}_x &= -\hat{a}x_s + \hat{b}y_s z_s + \hat{a}x_m - \hat{a}x_m + \hat{b}y_m z_m \\
&\quad - \hat{b}y_m z_m + ax_m - by_m z_m + u_x \\
&= -\hat{a}x_s + \hat{a}x_m + \hat{b}y_s z_s - \hat{b}y_m z_m - \hat{a}x_m \\
&\quad + ax_m + \hat{b}y_m z_m - by_m z_m + u_x \\
&= -\hat{a}(x_s - x_m) + \hat{b}(y_s z_s - y_m z_m) \\
&\quad - x_m(\hat{a} - a) + y_m z_m\left(\hat{b} - b\right) + u_x \\
&= -\hat{a}e_x + \hat{b}(y_s z_s - y_m z_m) - x_m e_a + y_m z_m e_b + u_x
\end{aligned}
\tag{25}
$$

In $\dot{e}_y$, add and subtract $-\hat{c}y_s^3$ and $\hat{d}x_s z_s$

$$
\begin{aligned}
\dot{e}_y &= -\hat{c}y_s^3 + \hat{d}x_s z_s - \hat{c}y_m^3 + \hat{c}y_m^3 + \hat{d}x_m z_m - \hat{d}x_m z_m \\
&\quad + cy_m^3 - dx_m z_m + u_y \\
&= -\hat{c}y_s^3 + \hat{c}y_m^3 + \hat{d}x_s z_s - \hat{d}x_m z_m - \hat{c}y_m^3 + cy_m^3 \\
&\quad + \hat{d}x_m z_m - dx_m z_m + u_y \\
&= -\hat{c}\left(y_s^3 - y_m^3\right) + \hat{d}(x_s z_s - x_m z_m) - y_m^3(\hat{c} - c) \\
&\quad + x_m z_m\left(\hat{d} - d\right) + u_y \\
&= -\hat{c}(y_s - y_m)\left(y_s^2 + y_s y_m + y_m^2\right) + \hat{d}(x_s z_s - x_m z_m) \\
&\quad - y_m^3 e_c + x_m z_m e_d + u_y \\
&= -\hat{c}e_y\left(y_s^2 + y_s y_m + y_m^2\right) + \hat{d}(x_s z_s - x_m z_m) \\
&\quad - y_m^3 e_c + x_m z_m e_d + u_y
\end{aligned}
\tag{26}
$$

In $\dot{e}_z$, add and subtract $\hat{e}z_m$, $-\hat{f}x_m y_m$, and $\hat{p}\tanh(y_m + g)$

$$
\begin{aligned}
\dot{e}_z &= \hat{e}z_s - \hat{f}x_s y_s + \hat{e}z_m - \hat{e}z_m - \hat{f}x_m y_m \\
&\quad + \hat{f}x_m y_m + \hat{p}\tanh(y_m + g) \\
&\quad - \hat{p}\tanh(y_m + g) + \hat{p}\tanh(y_s + g) - ez_m \\
&\quad + fx_m y_m - p\tanh(y_m + g) + u_z \\
&= \hat{e}z_s - \hat{e}z_m - \hat{f}x_s y_s + \hat{f}x_m y_m + \hat{e}z_m \\
&\quad - ez_m - \hat{f}x_m y_m + fx_m y_m + \hat{p}\tanh(y_m + g) \\
&\quad - p\tanh(y_m + g) - \hat{p}\tanh(y_m + g) \\
&\quad + \hat{p}\tanh(y_s + g) + u_z \\
&= \hat{e}(z_s - z_m) - \hat{f}(x_s y_s - x_m y_m) + z_m(\hat{e} - e) \\
&\quad - x_m y_m\left(\hat{f} - f\right) + \tanh(y_m + g)(\hat{p} - p) \\
&\quad - \hat{p}\tanh(y_m + g) + \hat{p}\tanh(y_s + g) + u_z \\
&= \hat{e}e_z - \hat{f}(x_s y_s - x_m y_m) + z_m e_e - x_m y_m e_f \\
&\quad + \tanh(y_m + g)e_p - \hat{p}\tanh(y_m + g) \\
&\quad + \hat{p}\tanh(y_s + g) + u_z
\end{aligned}
\tag{27}
$$

Finally, error dynamics can be written as

$$
\begin{aligned}
\dot{e}_x &= -\hat{a}e_x + \hat{b}(y_s z_s - y_m z_m) - x_m e_a + y_m z_m e_b + u_x \\
\dot{e}_y &= -\hat{c}e_y\left(y_s^2 + y_s y_m + y_m^2\right) + \hat{d}(x_s z_s - x_m z_m) \\
&\quad - y_m^3 e_c + x_m z_m e_d + u_y \\
\dot{e}_z &= \hat{e}e_z - \hat{f}(x_s y_s - x_m y_m) + z_m e_e - x_m y_m e_f \\
&\quad + \tanh(y_m + g)e_p \\
&\quad - \hat{p}\tanh(y_m + g) + \hat{p}\tanh(y_s + g) + u_z
\end{aligned}
\tag{28}
$$

Controller design

The controller design is performed in two steps

1. Constructing a sliding surface which presents the desired dynamics.
2. Selecting the switching control law to verify sliding condition.[42]

The integral sliding surface[41] can be written as

$$s_i = e_i + k_i \int e_i(\tau)d\tau \tag{29}$$

where $i = x, y, z$ and $k_i > 0$

The time derivative of the sliding surface is given by

$$\dot{s}_x = \dot{e}_x + k_x e_x \tag{30}$$

The parameter estimation errors are

$$
\begin{aligned}
e_a &= \hat{a} - a \\
e_b &= \hat{b} - b \\
e_c &= \hat{c} - c \\
e_d &= \hat{d} - d \\
e_e &= \hat{e} - e \\
e_f &= \hat{f} - f \\
e_p &= \hat{p} - p
\end{aligned} \tag{31}
$$

Let the adaptive sliding mode controllers be

$$
\begin{aligned}
u_x &= \hat{a}e_x - \hat{b}(y_s z_s - y_m z_m) - \eta_x \mathrm{sgn}s_x - \rho_x s_x - k_x e_x \\
u_y &= \hat{c}e_y(y_s^2 + y_s y_m + y_m^2) - \hat{d}(x_s z_s - x_m z_m) \\
&\quad - \eta_y \mathrm{sgn}s_y - \rho_y s_y - k_y e_y \\
u_z &= -\hat{e}e_z + \hat{f}(x_s y_s - x_m y_m) + \hat{p}\tanh(y_m + g) \\
&\quad - \hat{p}\tanh(y_s + g) - \eta_z \mathrm{sgn}s_z - \rho_z s_z - k_z e_z
\end{aligned} \tag{32}
$$

Let the adaptive parameter estimations be

$$
\begin{aligned}
\dot{\hat{a}} &= s_x x_m - k_x e_a \\
\dot{\hat{b}} &= -s_x y_m z_m - k_x e_b \\
\dot{\hat{c}} &= s_y y_m^3 - k_y e_c \\
\dot{\hat{d}} &= -s_y x_m z_m - k_y e_d \\
\dot{\hat{e}} &= -s_z z_m - k_z e_e \\
\dot{\hat{f}} &= s_z x_m y_m - k_z e_f \\
\dot{\hat{p}} &= -s_z[\tanh(y_m + g)] - k_z e_p
\end{aligned} \tag{33}
$$

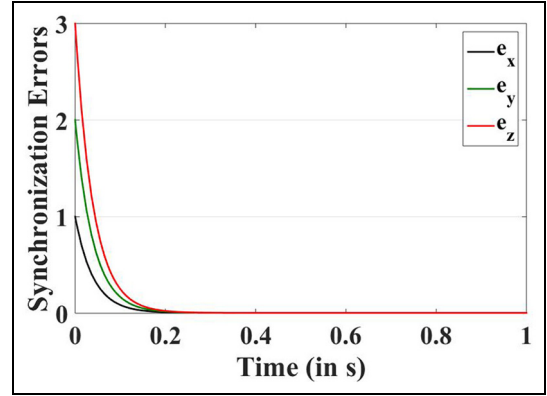To check the stability of the controlled system, let us consider the following Lyapunov candidate function

Figure 17. Time history of synchronization errors.

$$V = \frac{1}{2}\left[s_x^2 + s_y^2 + s_z^2 + e_a^2 + e_b^2 + e_c^2 + e_d^2 + e_e^2 + e_f^2 + e_p^2 \right] \tag{34}$$

The derivative of the Lyapunov function is given by

$$
\begin{aligned}
\dot{V} &= \dot{s}_x s_x + \dot{s}_y s_y + \dot{s}_z s_z + \dot{e}_a e_a + \dot{e}_b e_b + \dot{e}_c e_c \\
&\quad + \dot{e}_d e_d + \dot{e}_e e_e + \dot{e}_f e_f + \dot{e}_p e_p
\end{aligned} \tag{35}
$$

Substitute the controller in $\dot{V}$

$$
\begin{aligned}
\dot{V} &= s_x[-\eta_x \mathrm{sgn}s_x - \rho_x s_x] + s_y\left[-\eta_y \mathrm{sgn}s_y - \rho_y s_y\right] \\
&\quad + s_z[-\eta_z \mathrm{sgn}s_z - \rho_z s_z] \\
&\quad + e_a[\dot{\hat{a}} - s_x x_m] + e_b[\dot{\hat{b}} - s_x y_m z_m] + e_c[\dot{\hat{c}} - s_y y_m^3] \\
&\quad + e_d[\dot{\hat{d}} + s_y x_m z_m] \\
&\quad + e_e[\dot{\hat{e}} + s_z z_m] + e_f[\dot{\hat{f}} - s_z x_m y_m] \\
&\quad + e_p[\dot{\hat{p}} + s_z(\tanh(y_m + g))]
\end{aligned} \tag{36}
$$

Substitute the adaptive parameter estimation in $\dot{V}$

$$\dot{V} = -\eta_i|s_i| - \rho_i s_i^2 \tag{37}$$

where $i = x, y, z$

$$
\begin{aligned}
\dot{V} &= s_x\left[-\hat{a}e_x + \hat{b}(y_s z_s - y_m z_m) - x_m e_a + y_m z_m e_b + u_x + k_x e_x\right] \\
&\quad + s_y\left[-\hat{c}e_y^3 + \hat{d}(x_s z_s - x_m z_m) - y_m^3 e_c + x_m z_m e_d + u_y + k_y e_y\right] \\
&\quad + s_z\left[\begin{aligned}&\hat{e}e_z - \hat{f}(x_s y_s - x_m y_m) + z_m e_e - x_m y_m e_f + \tanh(y_m + g)e_p \\ &-\hat{p}\tanh(y_m + g) + \hat{p}\tanh(y_s + g) + u_z\end{aligned}\right] \\
&\quad + e_a[\dot{\hat{a}}] + e_b[\dot{\hat{b}}] + e_c[\dot{\hat{c}}] + e_d[\dot{\hat{d}}] + e_e[\dot{\hat{e}}] + e_f[\dot{\hat{f}}] + e_p[\dot{\hat{p}}]
\end{aligned} \tag{38}
$$

Introducing the parameter update law and the adaptive sliding mode controllers in equation (38), we get the Lyapunov first derivative as
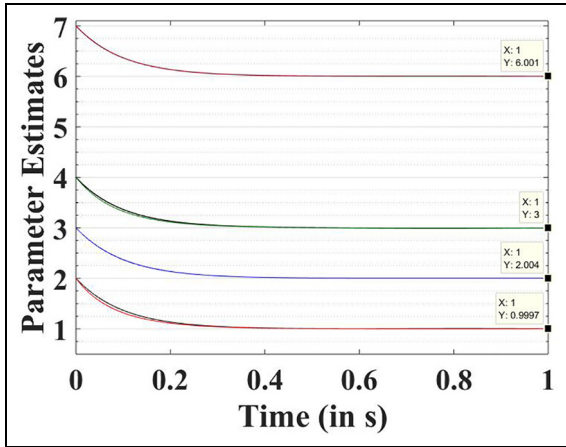
Figure 18. Time history of parameter estimates.

$$\dot{V} = -\eta_x |s_x| - \eta_y |s_y| - \eta_z |s_z| - \rho_x s_x^2 - \rho_y s_y^2 - \rho_z s_z^2 \tag{39}$$

The Lyapunov first derivative is a negative semi-definite as $\rho_i > 0$ and $\eta_i > 0$, and the synchronization errors e_x, e_y, e_z converge exponentially to zero as $t \to \infty$.

Numerical simulation is carried out, and the synchronization errors and parameter estimates are presented against time in Figures 17 and 18.

FPGA implementation

In this section, we discuss the implementation of the system in FPGA using Xilinx (Vivado) system generator toolbox in Simulink. FPGA implementations of fractional-order chaotic oscillators are discussed in literature.[43,44] Figure 19 shows the 2D phase portraits of the system using Xilinx System Generator, and Figure 20 shows the Xilinx register-transfer level (RTL) schematics of the system using Kintex 7. Comparing Figure 9 with Figure 19, one can clearly see that the FPGA-implemented system exhibits the same phase portraits for the initial conditions [0.1, 0.1, 0.6].

Step size is taken as $h = 0.001$, and the commensurate fractional order for implementing the system in FPGA is taken as $q = 0.99$. Figure 21 shows the power consumption chart of the FPGA implemented on fractional-order system, and the resources utilized are provided in Table 1.

Conclusion

The article investigated a chaotic system with cubic nonlinearity and hyperbolic function. The influence of the hyperbolic function is elaborately discussed. The integer order treatment and its dynamical properties are studied and confirm the bistability, multiscroll, and symmetric properties. Using G-L method, the system is
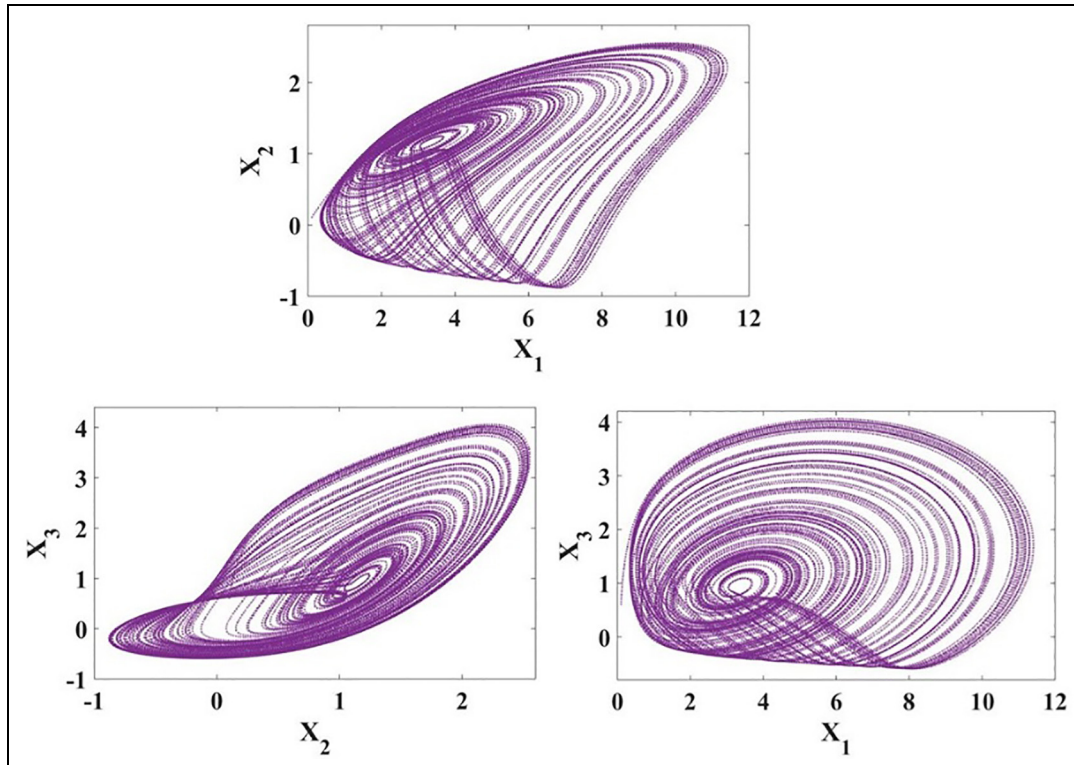

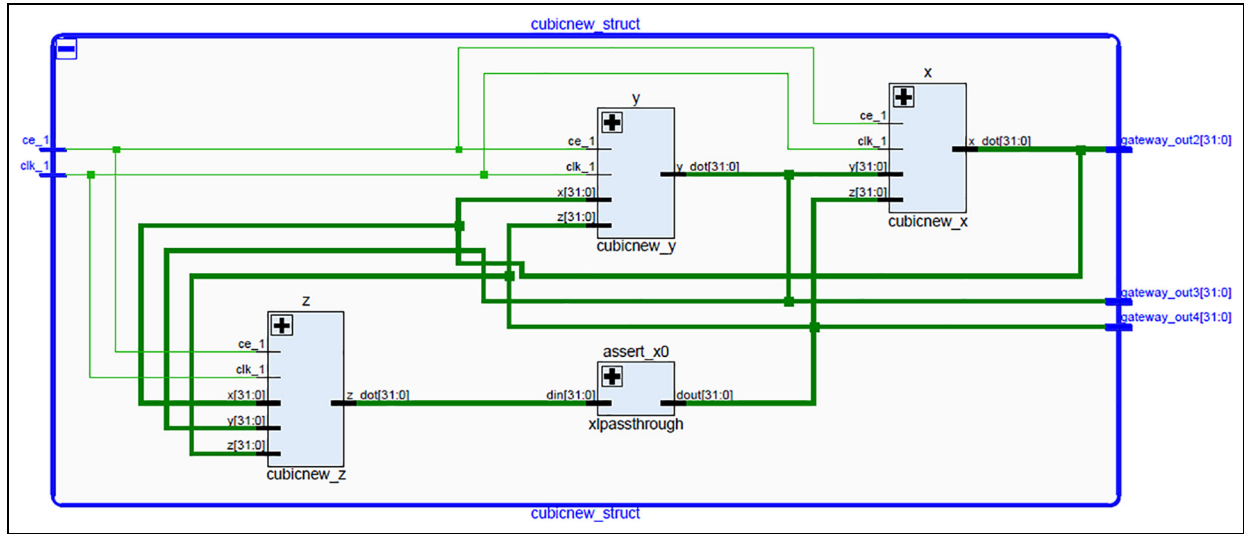**Figure 19.** 2D phase portrait of the system implemented in FPGA.

Figure 20. RTL schematics of the system implemented in FPGA.

Table 1. Resource utilization of the FO system implemented in FPGA.

Resource	Utilization	Available	Utilization %
LUT	678	203,800	0.33
FF	192	407,600	0.05
DSP	20	840	2.38
IO	97	500	19.40
BUFG	1	32	3.13

FO: fractional order; FPGA: field-programmable gate array; LUT: lookup table; FF: flip flops; DSP: digital signal processor; IO: input-output; BUFG: global buffer.
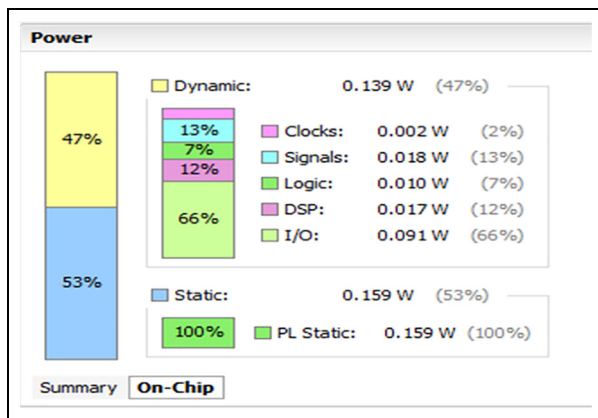

Figure 21. Power utilization of the FO system implemented in FPGA.

converted into fractional-order system. The numerical simulations for various order "*q*" are studied and confirmed that the above-said properties still remain in the system. Interestingly, by means of varying the order,

we could achieve the discussed properties. This shows the intricacy of the system and finds its application in secure communication. Adaptive synchronization of the system using sliding mode control scheme is presented. For implementing the fractional-order system in FPGA, Adomian decomposition method is used and the RTL schematic of the system is presented. Circuit realization would be carried out as a future work.

Declaration of conflicting interests

The author(s) declared no potential conflicts of interest with respect to the research, authorship, and/or publication of this article.

Funding

The author(s) received no financial support for the research, authorship, and/or publication of this article.

ORCID iD

B Lakshmi https://orcid.org/0000-0001-7862-2975

References

1. Wei Z, Moroz I, Sprott JC, et al. Detecting hidden chaotic regions and complex dynamics in the self-exciting homopolar disc dynamo. *Int J Bifurcat Chaos* 2017; 27: 1730008.
2. Wei Z, Pham V-T, Kapitaniak T and Wang Z. Bifurcation analysis and circuit realization for multiple-delayed Wang-Chen system with hidden chaotic attractors. *Nonlinear Dynam* 2016; 85: 1635–1650.
3. Wei Z, Moroz I, Wang Z, et al. Dynamics at infinity, degenerate Hopf and zero-Hopf bifurcation for Kingni-Jafari system with hidden attractors. *Int J Bifurcat Chaos* 2016; 26: 1650125.

4. Wei Z, Yu P, Zhang W, et al. Study of hidden attractors, multiple limit cycles from Hopf bifurcation and boundedness of motion in the generalized hyperchaotic Rabinovich system. *Nonlinear Dynam* 2015; 82: 131–141.

5. Wei Z, Sprott JC and Chen H. Elementary quadratic chaotic flows with a single non-hyperbolic equilibrium. *Phys Lett A* 2015; 379: 2184–2187.

6. Wei Z, Zhang W and Yao M. On the periodic orbit bifurcating from one single non-hyperbolic equilibrium in a chaotic jerk system. *Nonlinear Dynam* 2015; 82: 1251–1258.

7. Özkaynak F. Cryptographically secure random number generator with chaotic additional input. *Nonlinear Dynam* 2014; 78: 2015–2020.

8. Lu J and Chen G. Generating multiscroll chaotic attractors: theories, methods and applications. *Int J Bifurcat Chaos* 2006; 16: 775–858.

9. Lü J, Yu S, Leung H, et al. Experimental verification of multidirectional multiscroll chaotic attractors. *IEEE T Circuits-I* 2006; 53: 149–165.

10. Tang WKS, Zhong GQ, Chen G, et al. Generation of n-scroll attractors via sine function. *IEEE T Circuits-I* 2001; 48: 369–1372.

11. Yu S, Lü J and Chen G. A module-based and unified approach to chaotic circuit design and its applications. *Int J Bifurcat Chaos* 2007; 17: 1785–1800.

12. Yu S, Lü J, Leung H, et al. Design and implementation of n-scroll chaotic attractors from a general Jerk circuit. *IEEE T Circuits-I* 2005; 52: 1459–1476.

13. Lin Y, Wang C and Zhou L. Generation and implementation of grid multiscroll hyperchaotic attractors using CCII + . *Optik* 2016; 127: 2902–2906.

14. Yu S and Tang WKS. Generation of $n \times m$-scroll attractors in a two-port RCL network with hysteresis circuit. *Chaos Soliton Fract* 2009; 39: 821–830.

15. Lü J, Han F, Yu X, et al. Generating 3-D multi-scroll chaotic attractors: a hysteresis series switching method. *Automatica* 2004; 40: 1677–1687.

16. Suykens JAK and Vandewalle J. Generation of n-double scrolls (n = 1, 2, 3, 4,…). *IEEE T Circuits-I* 1993; 40: 861–867.

17. Li CL, Yu SM and Luo XS. A ring-scroll Chua system. *Int J Bifurcat Chaos* 2013; 23: 1350170.

18. Qi GY, Chen GR, Du SZ, et al. Analysis of a new chaotic system. *Physica A* 2005; 352: 295–308.

19. Ontañón-García LJ, Jiménez-López E and Campos-Cantón E. Generation of multiscroll attractors by controlling the equilibria. *IFAC Proc Vols* 2012; 45: 111–114.

20. Wang Y, Wang C and Zhou L. A time-delayed hyperchaotic system composed of multi-scroll attractors with multiple positive Lyapunov exponents. *J Comput Nonlin Dyn* 2017; 12: 051029.

21. Salama KN, Ozoguz S and Elwakil AS. Generation of n-scroll chaos using nonlinear transconductors. *IEEE Int Symp Circ S* 2003; 3: 176–179.

22. Sun K, Ai X and He S. Design of multi-scroll hyperchaotic system and analysis on its characteristic. *J Cent South Univ* 2015; 46: 1663–1672.

23. Radwan AG and Abd-El-Hafiz SK. The effect of multi-scrolls distribution on image encryption. In: *21st IEEE international conference on electronics, circuits and systems (ICECS)*, Marseille, France, 7–10 December 2014. New York: IEEE.

24. Günay E and Altun K. Multi-scroll chaotic attractors in SC-CNN via hyperbolic tangent function. *Electronics* 2018; 7: 67.

25. Rajagopal K, Karthikeyan A, Duraisamy P, et al. Bifurcation and chaos in integer and fractional order two-degree-of-freedom shape memory alloy oscillators. *Complexity* 2018; 2018: 8365845.

26. Ahmad W. Generation and control of multi-scroll chaotic attractors in fractional order systems. *Chaos Soliton Fract* 2005; 25: 727–735

27. Chen F. A Fractional-order Multi-scroll Chaotic System. *J Inform Comput Sci* 2013; 10: 1203–1211.

28. Ahmad W and Sprott JC. Chaos in fractional-order autonomous nonlinear systems. *Chaos Soliton Fract* 2003; 16: 339–351.

29. Flores-Vergara A, Inzunza-González E, García-Guerrero EE, et al. Implementing a chaotic cryptosystem by performing parallel computing on embedded systems with multiprocessors. *Entropy* 2019; 21: 268.

30. Flores-Vergara A, García-Guerrero EE, Inzunza-González E, et al. Implementing a chaotic cryptosystem in a 64-bit embedded system by using multiple-precision arithmetic. *Nonlinear Dynam* 2019; 96: 497–516.

31. Rodriguez-Orozco E, García-Guerrero EE, Inzunza-González E, et al. FPGA-based chaotic cryptosystem by using voice recognition as access key. *Electronics* 2018; 7: 414.

32. Jahanshahi H, Rajagopal K, Akgul A, et al. Complete analysis and engineering applications of a megastable nonlinear oscillator. *Int J Nonlin Mech* 2018; 107: 126–136.

33. Zhang M and Han Q. Dynamic analysis of an autonomous chaotic system with cubic nonlinearity. *Optik* 2016; 127: 4315–4319.

34. Wolf A, Swift JB, Swinney HL, et al. Determining Lyapunov exponents from a time series. *Physica D* 1985; 16: 285–317.

35. Baleanu D, Diethelm K, Scalas E, et al. *Fractional calculus: models and numerical methods*, vol. 5. Singapore: World Scientific, 2016.

36. Jafari S, Pham V-T and Kapitaniak T. Multiscroll chaotic sea obtained from a simple 3D system without equilibrium. *Int J Bifurcat Chaos* 2016; 26: 1650031.

37. Podlubny I. *Fractional differential equations: an introduction to fractional derivatives, fractional differential equations, to methods of their solution and some of their applications*, vol. 198. Amsterdam: Elsevier, 1998.

38. Li D, Chen WH, Wang Y, et al. Research on multi-scroll chaotic attractors synchronization technique. *Appl Mech Mater* 2014; 635–637: 1132–1135.

39. Li D and Ding GB. A new multi-scroll chaotic attractors synchronization technique. *Appl Mech Mater* 2012; 220–223: 1226–1229.

40. Vaidyanathan S and Sampath S. Sliding mode controller design for the global chaos synchronization of Coullet systems. In: Meghanathan N, Chaki N and Nagamalai D (eds) *Advances in computer science and information technology. Networks and communications* (Lecture notes of the institute for computer sciences, social informatics and

telecommunications engineering), vol. 84. Berlin: Springer, 2012, pp. 103–110.

41. Vaidyanathan S, Sampath S and Azar AT. Global chaos synchronisation of identical chaotic systems via novel sliding mode control method and its application to Zhu system. *Int J Model Identif Control* 2015; 23: 92–100.

42. Slotine J and Li W. *Applied nonlinear control*. Upper Saddle River, NJ: Prentice Hall, 1991.

43. Pano-Azucena AD, Ovilla-Martinezb B, Tlelo-Cuautlea E, et al. FPGA-based implementation of different families of fractional-order chaotic oscillators applying Grünwald–Letnikov method. *Commun Nonlinear Sci* 2019; 72: 51–527.

44. Tolba MF, AbdelAty AM, Soliman NC, et al. FPGA implementation of two fractional order chaotic systems. *AEU-Int J Electron C* 2017; 7: 162–172.